Center vortex model for the infrared sector of SU(3) Yang-Mills theory: Topological susceptibility

M. Engelhardt

Phys. Rev. D **83**, 025015 — Published 20 January 2011

DOI: 10.1103/PhysRevD.83.025015

Center vortex model for the infrared sector of SU(3) Yang-Mills theory: Topological susceptibility

M. Engelhardt[1]

Department of Physics, New Mexico State University
Las Cruces, NM 88003, USA

Abstract

The topological susceptibility of the $SU(3)$ random vortex world-surface ensemble, an effective model of infrared Yang-Mills dynamics, is investigated. The model is implemented by composing vortex world-surfaces of elementary squares on a hypercubic lattice, supplemented by an appropriate specification of vortex color structure on the world-surfaces. Topological charge is generated in this picture by writhe and self-intersection of the vortex world-surfaces. Systematic uncertainties in the evaluation of the topological charge, engendered by the hypercubic construction, are discussed. Results for the topological susceptibility are reported as a function of temperature and compared to corresponding measurements in $SU(3)$ lattice Yang-Mills theory. In the confined phase, the topological susceptibility of the random vortex world-surface ensemble appears quantitatively consistent with Yang-Mills theory. As the temperature is raised into the deconfined regime, the topological susceptibility falls off rapidly, but significantly less so than in $SU(3)$ lattice Yang-Mills theory. Possible causes of this deviation, ranging from artefacts of the hypercubic description to more physical sources, such as the adopted vortex dynamics, are discussed.

PACS: 12.38.Aw, 12.38.Mh, 12.40.-y
Keywords: Center vortices, infrared effective theory, confinement, topology

[1]email: engel@nmsu.edu

1 Introduction

A model of the QCD vacuum which has been successful in capturing the fundamental phenomena characterizing the strong interaction in its infrared, strongly coupled sector is the center vortex picture. It assumes that the long-wavelength modes of the gluon field are collectively organized into randomly distributed, percolating tubes of quantized chromodynamic flux in three-dimensional space; early in its development [1–12], this picture was often referred to, employing vivid imagery, as the "spaghetti vacuum". The aforementioned tubes of flux are termed "center vortices" since flux quantization is determined by the center of the underlying gauge group (detailed definitions are given in section 2.1). Contrary to spaghetti, vortices have no open ends; this is an expression of the Bianchi identity, i.e., continuity of flux (modulo Abelian magnetic monopoles). Also contrary to spaghetti, vortices can move through one another, i.e., their world-surfaces can intersect. The vortex picture, including its relation to other models of the QCD vacuum, has been reviewed in [13, 14].

While the vortex picture was originally conceived specifically as a possible mechanism of quark confinement, more recent developments have shown that it also provides viable explanations of the other two central phenomena observed in the low-energy sector of the strong interaction, namely, the spontaneous breaking of chiral symmetry and the axial $U_A(1)$ anomaly (the latter representing the focus of the study presented here). The vortex picture thus provides a comprehensive, consistent account of the gross features of the strong interaction vacuum. Two main lines of investigation have contributed to these developments. On the one hand, sparked by the inception of practicable algorithms for the detection of vortices in lattice Yang-Mills configurations [15–17], lattice studies of the vortex content of Yang-Mills theory and the effects it induces were carried out [15–23]. On the other hand, an infrared effective model based directly on center vortex degrees of freedom with a simplified effective dynamics was introduced to complement the lattice studies and expand on the range of vortex physics that could be accessed quantitatively [24–31].

In the lattice Yang-Mills approach, identifying center vortices within lattice configurations containing the full Yang-Mills dynamics is a complex pattern recognition problem. While center vortices are, in principle, defined gauge-invariantly via their effect on Wilson loops, cf. section 2.1, this pattern recognition problem is usually handled by adopting particular gauges which facilitate projecting out the vortex content of a given configuration. Two classes of gauges which have been employed in this respect are maximal center gauges [15, 16] and Laplacian center gauges [17]. On the basis of these methods, lattice Yang-Mills studies have demonstrated center dominance, i.e., that the vortex content of lattice Yang-Mills configurations fully accounts for the asymptotic string tension, both at zero temperature [15–17] and at finite temperatures [18]; the deconfining phase transition is revealed as a percolation transition (in certain three-dimensional slices of space-time) in the vortex picture [18]. Moreover, vortices account for the topological content of the Yang-Mills ensemble [19, 20]. The study of the chiral symmetry breaking

effects induced by vortices via the low-lying modes of the Dirac operator has proven to be technically more challenging due to the fact that center vortex configurations projected from full lattice Yang-Mills configurations are not smooth; nevertheless, it has been shown that chiral symmetry breaking disappears (along with topological charge and confinement) when vortices are removed from the full lattice configurations [17, 19], and a detailed study employing asqtad quarks [21] has demonstrated the emergence of a dense low-lying Dirac eigenvalue spectrum in the ensemble of vortex configurations projected from their full Yang-Mills counterparts.

These findings have been complemented by further recent investigations focusing on correlations between center vortices and low-lying overlap Dirac operator eigenmodes [21–23], which, on the other hand, can be tied to the topological charge density. Of related interest are studies of the connection between center vortices and other topological charge carriers arising in Yang-Mills theory; a detailed analysis of the vortex content of calorons was presented recently in [32]. Finally, a more formal issue which arises where correlations between center vortices and Dirac operator eigenmodes are concerned is the form of the index theorem in the presence of vortices; the non-smoothness of vortex gauge fields already alluded to further above may introduce complications in this respect. This has been investigated recently in [33, 34]. Some observations on the related question of the quantization properties of global topological charge are made below in section 3.3.

As already indicated, the lattice Yang-Mills studies of vortex physics highlighted above have been complemented by the formulation of a corresponding infrared effective model of center vortices. Since vortices represent lines of chromodynamic flux in three space dimensions, they correspondingly are described by two-dimensional world-surfaces in four-dimensional space-time. Implementing the notion that center vortices are randomly distributed, a random vortex world-surface model in Euclidean space-time was introduced and studied in [24–31]. Concentrating initially on an underlying $SU(2)$ gauge group, the confinement properties, including the finite temperature phase transition to a deconfined phase [24], the topological susceptibility [25] and the (quenched) chiral condensate [26] were found to quantitatively reproduce the corresponding features in $SU(2)$ lattice Yang-Mills theory. Subsequently, the model was generalized to other gauge groups, the confinement properties being investigated not only for the $SU(3)$ case [27–29], but also for $SU(4)$ [30] and $Sp(2)$ [31]. For the most relevant case of an underlying $SU(3)$ gauge group, a weakly first order deconfinement transition [27, 29] and a Y-law for the baryonic static potential [28] were found, in accordance with $SU(3)$ lattice Yang-Mills theory. The present work continues the investigation of the $SU(3)$ model, focusing on the topological susceptibility, which is instrumental in determining, via the axial $U_A(1)$ anomaly, the mass of the η' meson. Preliminary accounts of this work have been given in [35, 36].

2 Modeling center vortices

2.1 Center vortex degrees of freedom

The vortex picture of the strong interaction vacuum assumes that the relevant infrared gluonic degrees of freedom are center vortices. On infrared length scales, center vortices are closed lines of quantized chromomagnetic flux in three space dimensions. They are therefore described by closed two-dimensional world-surfaces in four-dimensional space-time. Their flux is quantized according to the center of the gauge group; if one evaluates a Wilson loop W encircling an $SU(3)$ vortex flux, one obtains one of the nontrivial[2] center elements of the $SU(3)$ group, i.e.,

$$W = \exp(\pm 2\pi i/3) \; . \tag{1}$$

Note that the two center elements in question are complex conjugates of one another, implying that the $SU(3)$ gauge group only really allows for one type of vortex flux, the two possible space-time orientations of which determine which center element is measured.

Note furthermore that the specific structure of the $SU(3)$ center also allows for vortex branching. A vortex flux associated with $W = \exp(2\pi i/3)$ branching into two vortex fluxes each associated with $W = \exp(-2\pi i/3)$ is compatible with the Bianchi constraint, i.e., flux continuity modulo Abelian magnetic monopoles; evaluating a Wilson loop encircling the latter two fluxes yields $W = \exp(-2\pi i/3) \cdot \exp(-2\pi i/3) = \exp(2\pi i/3)$, just as for the original flux.

Viewing center vortices as infrared effective degrees of freedom implies that their space-time location is only determined to an accuracy limited by the ultraviolet cutoff. Equivalently, if one sufficiently increases the space-time resolution, it is appropriate to represent center vortices as thickened tubes in three space dimensions, or correspondingly thickened world-surfaces in space-time. This thickness, encoding the ultraviolet cutoff, is relevant for medium-range phenomena such as Casimir scaling of the static quark potential at intermediate distances [37, 38]. It plays a role in the construction of an infrared effective vortex dynamics, cf. section 4.1.

2.2 Vortex field strength

To evaluate the topological charge

$$Q = \frac{1}{32\pi^2} \int d^4x \, \epsilon_{\mu\nu\lambda\tau} \; \mathrm{Tr} \; F_{\mu\nu} F_{\lambda\tau} \tag{2}$$

of center vortices, it is necessary to associate a chromodynamic field strength tensor $F_{\mu\nu}$ with them. While it will not be necessary to give a general construction of $F_{\mu\nu}$ for an

[2] Of course, the trivial unit center element signals that no flux is present.

arbitrary vortex configuration [39], a few of its properties need to be specified for the developments further below.

A vortex world-surface element running in the ρ and σ directions carries a field strength $F_{\mu\nu}$, localized on the world-surface, such that the μ and ν directions are perpendicular to the ρ and σ directions [25,39]. Apart from this gauge-invariant statement, the field strength also has a direction in color space, which can be rotated by gauge transformations. It is convenient to cast vortex configurations in an Abelian gauge, i.e., the 3×3 color matrix $F_{\mu\nu}$ will be chosen diagonal. Vortex color structure can be usefully characterized by eliminating the space-time details of the vortex field strength and considering only the color direction $T(r)$ of the vortex at the position r,

$$\frac{2\pi}{3} T(r) = \frac{1}{2} \int_{S_r} F_{\mu\nu} \, d^2 S_{\mu\nu} = \int_{\partial S_r} A_\mu \, dx_\mu \ , \tag{3}$$

where S_r is a two-dimensional surface intersecting the vortex at r (but intersecting no other fluxes) and A_μ is a (diagonal) gauge field generating the field strength $F_{\mu\nu}$. In terms of a parametrization $x(s_1, s_2)$ of S_r, the oriented surface element is given by $d^2 S_{\mu\nu} = \epsilon_{\kappa\lambda} (\partial x_\mu / \partial s_\kappa)(\partial x_\nu / \partial s_\lambda) ds_1 ds_2$. In terms of T, the Wilson loop along the contour ∂S_r encircling the vortex is simply given by

$$W = \frac{1}{3} \, \mathrm{Tr} \, \exp(2\pi i T/3) \ , \tag{4}$$

i.e., T has integer entries. As one travels along the vortex world-surface, T remains constant except possibly at lines on the surface at which T switches from one color direction to another, in a manner which must of course be compatible with the Bianchi constraint. In fact, such switches in the color direction T are unavoidable on generic vortex world-surfaces. In the simpler case of an $SU(2)$ gauge group [25], this comes about purely due to the nonorientability of the surfaces. Nonorientability implies that there must be lines on the surfaces at which the orientation of vortex flux is inverted and T therefore displays a discontinuity. In the $SU(3)$ case considered here, the picture is complicated by the branched nature of the surfaces, cf. further below. Moreover, while in the $SU(2)$ case, the choice of the set of allowed color directions T is essentially unique, in the $SU(3)$ case, one has a certain amount of (gauge) freedom in the choice of the set of allowed color directions. These options, leading to different patterns of discontinuities on the vortex world-surfaces, will be discussed further in the next section.

In more physical terms, a discontinuity in the color direction of vortex flux described by T implies the presence of a source or sink of that flux, i.e., the presence of an Abelian magnetic monopole world-line on the vortex world-surface. In view of the fact that such discontinuities in general cannot be avoided, Abelian magnetic monopoles represent intrinsic features of vortex configurations cast in Abelian gauges. This is, of course, the character of Abelian gauges; rotations of the field strength tensor in color space, which in general occur continuously as a function of space-time location, are compressed into

singular jumps. The precise locations of the monopole world-lines on the vortex world-surfaces can be shifted by gauge transformations, but certain topological characteristics of these singularities are gauge-invariant (they are, e.g., in general non-contractible), and influence, in particular, the topological charge[3].

2.3 Vortex color structure

As indicated above, for the $SU(3)$ gauge group, one has different options in the choice of the set of allowed color directions T on vortex world-surfaces, corresponding to a residual freedom in the choice of Abelian gauge. Consider, to begin with, a minimal set, i.e., let

$$T \in \{\pm \,\mathrm{diag}(1,1,-2)\} \ . \tag{5}$$

This is sufficient to generate both nontrivial center elements of the $SU(3)$ group, cf. (1), i.e., both possible orientations of vortex flux. Consider now the occurrence of monopoles. Contrary to the $SU(2)$ case [25], in this description, monopoles cannot occur away from branchings, since the flux required to switch from $T = \mathrm{diag}(1,1,-2)$ to $T = \mathrm{diag}(-1,-1,2)$ does not correspond to a possible Abelian magnetic monopole flux (which would be described by diagonal elements which are integer multiples of 3 in the convention used here). On the other hand, monopoles *must* occur at branchings, cf. Fig. 1.

Consider, on the other hand, a non-minimal, more symmetric choice,

$$T \in \{\pm \,\mathrm{diag}(1,1,-2), \pm \,\mathrm{diag}(1,-2,1), \pm \,\mathrm{diag}(-2,1,1)\} \ . \tag{6}$$

This description, introduced in [40–42], allows for more flexibility; monopoles can occur away from branchings, cf. Fig. 2, and branchings are not necessarily associated with monopoles, cf. Fig. 3. In fact, this description affords the possibility of deforming monopole world-lines such that they never coincide with vortex world-surface branching lines, except for, at most, isolated crossings of the former and the latter. This property singles out the choice (6) as the one best suited for the purpose of evaluating the topological charge of $SU(3)$ vortex configurations, cf. section 3.2.

2.4 Vortex world-surfaces on a hypercubic lattice

In order to arrive at a practical scheme of generating model vortex world-surface ensembles, cf. section 4.1, the world-surfaces will be composed of elementary squares on a hypercubic lattice. One can then describe a vortex configuration by recording the chromodynamic flux associated with each elementary square in the lattice. Associate the lattice elementary square extending from the lattice site x into the positive μ and ν directions with a 3×3 color matrix $p_{\mu\nu}(x)$, where either $p_{\mu\nu}(x) = 0$ (indicating the

[3]Indeed, on a torus with periodic boundary conditions (nontrivial boundary conditions such as torus twist require additional consideration), globally oriented vortex world-surfaces, i.e., ones devoid of monopoles, carry no global topological charge [39].

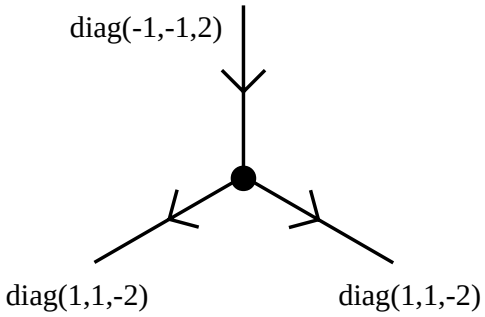

Figure 1: Vortex color structure at branchings for a minimal choice of the set of allowed color generators T, cf. (5). The restricted set of available T forces a monopole to appear at the branching; the difference between incoming and outgoing fluxes is $\mathrm{diag}(-1,-1,2) - 2\cdot\mathrm{diag}(1,1,-2) = \mathrm{diag}(-3,-3,6) = \mathrm{diag}(-3,0,3) + \mathrm{diag}(0,-3,3)$, i.e., monopole flux which can be further decomposed into two elementary monopoles in two separate $SU(2)$ subgroups of $SU(3)$, as indicated by the second equality.

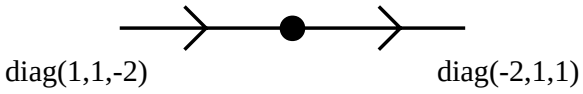

Figure 2: Possible monopole not associated with branching for a non-minimal choice of the set of allowed color generators T, cf. (6). The difference between incoming and outgoing fluxes is $\mathrm{diag}(1,1,-2) - \mathrm{diag}(-2,1,1) = \mathrm{diag}(3,0,-3)$, i.e., a monopole flux.

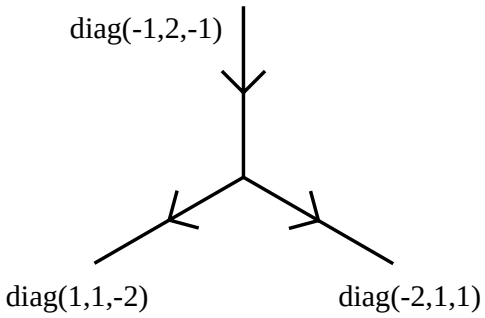

Figure 3: Possible vortex color structure at branchings for a non-minimal choice of the set of allowed color generators T, cf. (6). One can choose incoming and outgoing fluxes such that their difference vanishes, $\mathrm{diag}(-1,2,-1) - \mathrm{diag}(1,1,-2) - \mathrm{diag}(-2,1,1) = 0$. In this description, one thus has the freedom to disassociate monopoles from branchings.

absence of vortex flux) or $p_{\mu\nu}(x) = T$ with T indicating the color orientation of the vortex flux on the square in question, as introduced in the previous section, cf. (6). Note that the order of indices defines a sense of curl and, accordingly, $p_{\nu\mu}(x)$ and $p_{\mu\nu}(x)$ are related by space-time inversion, i.e., $p_{\nu\mu}(x) = -p_{\mu\nu}(x)$. In practice, it is thus sufficient to record $p_{\mu\nu}(x)$ for $\mu < \nu$.

An operation repeatedly used in the following is an *elementary cube transformation*, which locally deforms a given vortex world-surface configuration on the lattice into a new configuration as follows. An additional closed vortex flux, of the shape of the surface of an elementary three-dimensional cube (the smallest possible closed vortex world-surface), and associated with one of the possible color orientations T from (6), is superimposed onto the original configuration. This creates a new configuration while preserving the Bianchi constraint, i.e., continuity of flux modulo Abelian magnetic monopoles. Specifically, if the elementary cube in question extends from the lattice site x into the positive μ, ν and λ directions, the transformation effects

$$\begin{array}{ll} p_{\mu\nu}(x) \to \mathrm{Mod}\,(p_{\mu\nu}(x) + T)\,, & p_{\mu\nu}(x + e_\lambda) \to \mathrm{Mod}\,(p_{\mu\nu}(x + e_\lambda) - T) \\ p_{\nu\lambda}(x) \to \mathrm{Mod}\,(p_{\nu\lambda}(x) + T)\,, & p_{\nu\lambda}(x + e_\mu) \to \mathrm{Mod}\,(p_{\nu\lambda}(x + e_\mu) - T) \\ p_{\lambda\mu}(x) \to \mathrm{Mod}\,(p_{\lambda\mu}(x) + T)\,, & p_{\lambda\mu}(x + e_\nu) \to \mathrm{Mod}\,(p_{\lambda\mu}(x + e_\nu) - T) \end{array} \tag{7}$$

where Mod denotes a generalized modulo operation, acting on diagonal 3×3 color matrices, which maps its argument back into the set of allowed color orientations, cf. (6); it acts as follows:

$$\begin{array}{lll} \mathrm{Mod}(P) = 0 & \text{if} & \det P = 0 \\ \mathrm{Mod}(P) = -P/2 & \text{if} & |\det P| = 16 \\ \mathrm{Mod}(P) = P & \text{else} & \end{array} \tag{8}$$

Note that the first two alternatives in general induce Abelian magnetic monopole lines in the transformed configuration.

Elementary cube transformations will be employed further below both as Monte Carlo updates[4] in the generation of vortex world-surface ensembles, as well as in the process of measuring the topological charge.

3 Vortex topological charge

3.1 Origin of vortex topological charge density

The topological charge of vortex world-surfaces results from world-surface intersections and world-surface writhe [25, 39, 40, 43, 44]. If one considers idealized, infinitely thin

[4]Strictly speaking, purely as a matter of technical convenience, Monte Carlo updates will act directly on the reduced quantities $q_{\mu\nu}(x)$ introduced in (11), which carry only part of the information contained in $p_{\mu\nu}(x)$; the action is entirely analogous and can be unambiguously inferred from the definition given here.

surfaces in four-dimensional space-time, intersections occur at isolated points in space-time, whereas writhe in general is continuously distributed along surfaces. An illustrative example is given in [44]. In an infrared effective framework, where locations cannot be specified to higher accuracy than given by the ultraviolet cutoff, these features are smeared out over the corresponding length scale (which in practice can be identified with the vortex thickness).

On the other hand, if for modeling purposes one composes vortex world-surfaces from elementary squares on a hypercubic lattice, as will be done below, additional considerations must be taken into account. In such a setting, topological charge can only be generated at lattice sites, since these are the only space-time points at which surface elements can meet such that their tangent vectors span all four space-time dimensions[5]. Thus, also vortex writhe becomes concentrated on space-time points instead of being continuously distributed on vortex world-surfaces.

At first sight, it would therefore seem that the topological charge Q of hypercubic model surfaces can be evaluated simply by considering all lattice sites x, and at each site counting pairs of mutually orthogonal elementary squares meeting there, appropriately weighted by the associated chromodynamic flux,

$$Q = \sum_x q(x) \ , \qquad q(x) = \frac{1}{288} \sum_{\mu<\nu} \sum_{\lambda<\tau} \sum_{i,j=1}^{4} \epsilon_{\mu\nu\lambda\tau} \, \mathrm{Tr} \left(p_{\mu\nu}^{(i)} \, p_{\lambda\tau}^{(j)} \right) \tag{9}$$

where $p_{\mu\nu}^{(i)}$, $i = 1, \ldots, 4$ denotes the four elementary lattice squares touching the lattice site x and extending into the μ and ν directions. The normalization of $q(x)$ can be inferred by noting that vortex world-surface intersection points generate contributions of magnitude $1/3$ or $2/3$ to the topological charge [39] (depending on the relative color orientation of the surfaces). Note that, as written, each pair of elementary squares is counted twice as μ, ν, λ, τ are summed over; this is also properly taken into account by the normalization prefactor.

However, before a measurement of the topological charge according to (9) can be implemented, certain ambiguities in the surface configurations, engendered by the hypercubic construction, must first be resolved.

3.2 Ambiguities in measuring topological charge

There are two types of ambiguities which arise in defining the topological charge of hypercubic model surfaces. First, intersections of such surfaces do not necessarily occur only at space-time points, but they can be spread out into lines, as exemplified in Fig. 4. Contrast this with the generic intersections found for arbitrary continuous two-dimensional

[5]Recall that a vortex world-surface running in the ρ and σ directions is associated with a field strength $F_{\mu\nu}$ such that the μ and ν directions are perpendicular to the ρ and σ directions. Therefore, to generate a nonvanishing topological density $\epsilon_{\mu\nu\lambda\tau}$ Tr $F_{\mu\nu} F_{\lambda\tau}$, surface elements must meet such that their tangent vectors span all four space-time dimensions.

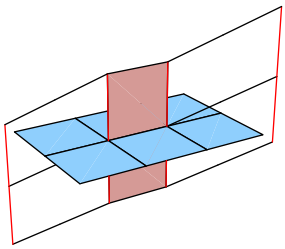

Figure 4: Vortex world-surfaces composed of elementary squares on a hypercubic lattice exhibit ambiguities, such as two or more surface segments meeting along a whole line, which do not arise in continuum random surface ensembles.

surfaces in four-dimensional space-time. In a generic ensemble of random continuous surfaces, situations such as depicted in Fig. 4, where two or more surfaces meet along a whole line (or, in the lattice language, where four or more elementary squares meet along a link) represent a set of measure zero. Instead, intersections occur only at points. In that case, one can unambiguously identify the two distinct participating surfaces, and, moreover, they will each have a well-defined orientation at the intersection, since monopole world-lines generally will not run exactly through the intersection point. This leads to a well-defined contribution to the topological charge.

By contrast, if an intersection point is spread out into a line, it can happen that a monopole line crosses the intersection line, implying that the surfaces intersecting do not possess unique orientations throughout the intersection region. One might contemplate deforming the monopole line around the intersection region, but it is unclear how to do so, because, in general, it is not even possible to unambiguously distinguish between the two surfaces which are intersecting in the first place. Given a vortex configuration in which four or more elementary squares meet along a link, there may be more than one way of assigning the squares in question to two distinct surfaces; different assignments may even lead to different conclusions as to whether an actual intersection point is observed or two surfaces are merely touching.

This ambiguity in identifying the two distinct surfaces participating in a situation where four or more vortex elementary squares meet along a lattice link must be resolved before a topological charge can be assigned. This is achieved by locally deforming the vortex world-surfaces until at most three vortex elementary squares meet at each lattice link (the case of three squares meeting, which does not occur in the $SU(2)$ model [25], constitutes a bona fide vortex branching allowed in the $SU(3)$ case studied here). In practice, the given world-surface configuration is placed on a finer lattice with 1/3 of the original lattice spacing, and one sweep is performed through the lattice, carrying out elementary cube transformations, cf. section 2.4, such as to eliminate lattice links with more than three vortex elementary squares attached. This is quite efficient in practice; almost all such ambiguities disappear on the first iteration of this algorithm, and only

one further iteration is necessary to completely eliminate residual cases and arrive at an unambiguous surface configuration. Thus, in practice, one ends up with a configuration on a lattice with 1/9 the original lattice spacing. Note that the algorithm only performs local deformations in the sense that the original surfaces are displaced by less than half of the original lattice spacing. The values of Wilson loops defined in the original configuration are thus manifestly unchanged. From the point of view of an infrared effective model, the local deformations performed are smaller than the uncertainty in defining vortex location implied by the ultraviolet cutoff. However, while the confinement properties of the ensemble are thus preserved, there is unfortunately the possibility of spurious additional contributions to the topological charge being introduced on the finer lattice scales (similar to the way instantons can "fall through the lattice" in standard lattice Yang-Mills theory). The corresponding systematic downward uncertainty in the measured topological susceptibility will be estimated, cf. section 5.2, via the simultaneous increase in vortex density caused by the algorithm, which turns out to be appreciable. This will in fact represent the chief uncertainty of the measurement.

The second ambiguity in hypercubic world-surface configurations which needs to be removed is associated with the structure of vortices in color space. In the hypercubic description, topological charge density is concentrated at lattice sites; on the other hand, also magnetic monopole world-lines are forced to run along lattice links, and, thus, through lattice sites. The coincidence of a singular concentration of topological charge with a magnetic monopole singularity is ambiguous. Contrast this again with the generic structures found for arbitrary continuous two-dimensional surfaces in four-dimensional space-time. In the case of an intersection point, random monopole world-lines on the vortex surface will generally pass by that exact point instead of going through it. In the case of vortex writhe, which is continuously distributed along continuous two-dimensional surfaces, a monopole world-line may indeed run through the region of writhe; however, this has a negligible effect on the topological charge density, for the following reason: Changing the color orientation T of a vortex surface segment leaves the topological charge density generated by writhe within that segment invariant. Thus, the only way in which a monopole world-line can influence topological charge density is through interference of field strengths located on different sides of the monopole. For thin surfaces, such interference is negligible; for thickened surfaces, the situation is not quite as clear-cut, cf. further comments below. Disregarding for the moment the complications implied by vortex thickness, the situation for continuous two-dimensional surfaces is therefore this: Topological charge density generated by vortex writhe is distributed continuously on the surface and insensitive to the presence of monopoles, except exactly at the location of the monopole world-line; however, when integrating the topological charge density, the monopole world-line region, being of lower dimensionality, has measure zero. This is different from the hypercubic case, where the lattice description forces the entire topological charge density to be concentrated at a lattice site, implying spurious finite interference terms between field strengths located on either side of a monopole world-

line. To faithfully model the behavior of the topological charge density of continuous vortex world-surfaces within the hypercubic construction employed here, one should therefore deform all magnetic monopole world-lines around lattice sites such that they never intersect points of nonvanishing topological charge density. Note that this can be, and is, effected locally and independently for each lattice site, once one adopts the choice (6) for the description of the color orientations possible for vortex world-surfaces. This is the point where the adoption of the choice (6) is crucial; it permits the resolution of the ambiguities associated with vortex color structure within the hypercubic construction of the vortex world-surfaces employed here. Further discussion of the choice of vortex color structure in the dynamical configurations contained in the random vortex world-surface ensemble follows below in section 4.2.

Returning to the case of thickened vortex world-surfaces deferred in the discussion above, in general, one can indeed construct configurations in which field strengths on different sides of a magnetic monopole may interfere and thereby generate a contribution to the topological charge density associated specifically with the monopole. An example of such a configuration is given in [42]. However, presumably, such contributions are merely taken into account at a different level once one adopts a construction in terms of thin world-surfaces. The connection between thick vortices and their idealized thin representatives is presumably topologically trivial, i.e., one can envisage continuously deforming thick chromodynamic fluxes into thin constrictions thereof; then, the topological charge density originally present in the thick flux would remanifest itself in additional writhe and self-intersection of the constricted flux. The further developments in the present work will base on this presumption, whether it represents an auxiliary model assumption or whether it indeed implies no loss of generality. Monopole lines will, as described further above, always be deformed such that space-time points with nonvanishing topological charge density are avoided; no separate topological charge density will be associated with magnetic monopole world-lines. In particular in the hypercubic description with the choice of allowed color orientations (6), monopoles can always be routed on the vortex world-surfaces such that all chromodynamic flux in their immediate surroundings is confined to three dimensions, i.e., cannot contribute to the topological charge density. It should be emphasized that, within the present vortex model, magnetic monopoles are not treated as separate physical degrees of freedom; rather, they are merely manifestations of the non-orientedness of the vortex world-surfaces arising in Abelian gauges such as implied by the choice (6). Accordingly, their exact space-time location has no physical significance to the extent that it can be varied by a change of gauge such that vortex world-surface color orientation is rotated within the set (6). While there are global constraints to such a change, implied, e.g., by nonorientability, cf. also a further discussion of gauge invariance in section 4.2, the local deformations necessary to remove all interactions between monopole world-lines and space-time points carrying topological charge density are always possible.

Figure 5: Magnetic monopoles present in a generic vortex configuration A (left, where the broken line indicates the Dirac string) are replaced by additional physical auxiliary fluxes in the corresponding configuration A' (right). The auxiliary flux can furthermore be decomposed into a superposition of coinciding vortex fluxes (depicted slightly displaced from one another in the right-hand panel for better visibility).

3.3 Remarks on topological charge quantization

The global topological charge Q of hypercubic model vortex world-surfaces with $SU(3)$ color, evaluated as described above, is quantized in half-integer units. The same property is exhibited in the $SU(2)$ case [25], cf. also recent related work reporting evidence for half-integer topological charge in a sample vortex configuration [34], as well as the example given in [26]. To understand this behavior, it should first be noted that vortex world-surfaces carrying global topological charge are not defined on smooth, simple manifolds. In the Abelian gauge language, a vortex configuration exhibiting nonvanishing global topological charge must be non-oriented, i.e., carry Abelian magnetic monopoles [39]. The magnetic monopoles imply the presence of Dirac string singularities in the vortex gauge field which must be excised from space-time. As a consequence, the manifold supporting the vortex gauge field acquires a complicated topology with internal boundaries, and topological charge is not necessarily quantized in the manner which is found on simple manifolds such as spheres or tori[6]. Indeed, the topology of the space-time manifold is dynamic, in close correspondence to the dynamic nature of the vortex topological charge.

To understand this correspondence in further detail, it is useful to associate with any given Abelian vortex gauge field configuration A a corresponding configuration A' defined as follows. Let A be identical to A' everywhere except at Dirac strings. Instead of excising Dirac string world-surfaces from space-time, let A' contain physical thin magnetic fluxes where A exhibits Dirac strings, cf. Fig. 5. These magnetic fluxes will be referred to as "auxiliary fluxes" in the following. The magnitudes of these auxiliary fluxes shall be multiples of 3 (in each diagonal color component, in the same convention as used for the color orientation matrices T introduced in section 2.3), such as to supply precisely the magnetic flux emanating from the magnetic monopoles in A.

[6]Note that this is not an artefact of the Abelian description; whereas one can indeed construct (singular) non-Abelian gauge transformations which eliminate Abelian magnetic monopoles and the associated Dirac strings [39], these transformations will not obey smooth boundary conditions at the external boundaries of the manifold. The singular behavior is merely shifted from internal boundaries in the region of the vortex carrying topological charge to the external boundaries, thus precluding compactification of the manifold at the latter to, say, a sphere or a torus.

The configuration A' thus has no sources or sinks of magnetic flux, i.e., magnetic monopoles, and no Dirac strings. Instead, at any point where vortex magnetic flux is discontinuous in A, in A', this flux is continuously carried away by the newly introduced auxiliary fluxes. Indeed, one can view all auxiliary fluxes as superpositions of additional vortex fluxes with coinciding[7] world-surfaces, cf. Fig. 5. Magnetic flux in A' is completely continuous, and A' is defined on a manifold with no internal boundaries. Consequently, its global topological charge vanishes [39].

This opens the possibility of quantifying the topological charge of A in an alternative manner, namely, via the properties of its Dirac strings, or, equivalently, the properties of the corresponding auxiliary fluxes in A'. Consider the ways in which the topological charge contributions found in A' differ from the ones found in A. Besides the vortex topological charge proper, as measured in A, A' contains the following additional contributions:

- Contributions from intersections between vortices and auxiliary fluxes, $Q[A \cap Aux]$. These generate integer topological charge contributions.
- Contributions from intersections of auxiliary fluxes with auxiliary fluxes, $Q_{int}[Aux]$. Also these generate integer topological charge contributions.
- Contributions from auxiliary flux writhe, $Q_{writhe}[Aux]$.

Note that, in accordance with the comments at the end of the previous section, additional contributions from flux writhe at the edges of the auxiliary fluxes, where the original configuration A displays monopoles, are not contemplated. Monopoles are always routed such that vortex flux in their immediate surroundings extends purely in three dimensions, and one can convince oneself that attaching auxiliary fluxes to lines routed in this fashion can also always be achieved such that no writhe contributing to the topological charge density results.

As a result of this construction, one can thus equate

$$0 = Q[A'] = Q[A] + Q[A \cap Aux] + Q_{int}[Aux] + Q_{writhe}[Aux] \ , \tag{10}$$

which implies that the quantization properties of $Q[A]$ are determined by the quantization properties of $Q_{writhe}[Aux]$ (given that $Q[A \cap Aux]$ and $Q_{int}[Aux]$ are integers). In this sense, there is a correspondence between the topology of the space-time manifold and the quantization of the topological charge of the vortex world-surfaces. Moreover,

[7]Note that for the present argument, auxiliary fluxes are not intended to be separated into non-coinciding vortex world-surfaces. While this would indeed constitute yet another legitimate point of view, it is not helpful in the present context, since it in general introduces additional topologically nontrivial features. For instance, in the slightly displaced depiction of Fig. 5 (right), consider connecting the two corners of the shown fluxes by an imaginary line segment; adding another dimension, this line segment becomes a band. Globally, this band may have the topology of a Möbius strip, which would imply additional writhe and self-intersection in the separated vortex fluxes. Such complications do not have to be taken into account if one foregoes separating the auxiliary fluxes into disjoint center vortex units.

it thus becomes plausible that this quantization is independent of the gauge group employed, as observed in practice and mentioned at the beginning of this section[8]. After all, the magnitudes of the auxiliary fluxes determining $Q_{writhe}[Aux]$ are independent of the gauge group[9], and consequently, it is plausible that also the quantization properties of $Q_{writhe}[Aux]$ (and, therefore, $Q[A]$) would be independent of the gauge group.

A caveat to this argument is the following: Whereas locally, the contributions to $Q_{writhe}[Aux]$ stemming from writhe and self-intersection of the auxiliary fluxes are indeed independent of the gauge group, globally, the topologies of the auxiliary flux world-surfaces differ. E.g., for $SU(3)$, auxiliary flux may branch, whereas it cannot for $SU(2)$. Now, in complete analogy to the argument used further above, excluding auxiliary flux writhe at the edges where auxiliary flux is attached to the physical vortices, one can also always configure $SU(3)$ auxiliary flux branching lines such that they do not carry writhe. Thus, both for $SU(2)$ and for $SU(3)$, $Q_{writhe}[Aux]$ is determined by writhe and self-intersections in the interior of open auxiliary flux world-surfaces, with the only difference that, in the $SU(3)$ case, the edges of the open world-surfaces include not only the lines where the auxiliary flux is attached to the physical vortices, but may also include auxiliary flux branching lines. It thus remains plausible that $Q_{writhe}[Aux]$ is quantized in the same way for both gauge groups. Nevertheless, at this point there is no stringent argument excluding the possibility that global space-time constraints may induce differences in the available sets of open auxiliary flux world-surfaces for the two gauge groups. As a result, the above observations, motivating the coinciding topological charge quantization properties of $SU(2)$ and $SU(3)$ model center vortices, should be taken as no more than an a posteriori plausibility argument.

4 Vortex ensemble

4.1 Dynamics

The dynamics of the $SU(3)$ random vortex world-surface model were constructed and discussed in detail in [27]. Vortex world-surfaces are composed of elementary squares on a hypercubic lattice, as described in section 2.4. An ensemble of random vortex world-surfaces is generated via Monte Carlo methods, where preservation of the Bianchi constraint (continuity of flux modulo Abelian magnetic monopoles) is guaranteed by using the elementary cube transformations of section 2.4 as the elementary updates. The ensemble is weighted by an action penalizing curvature of vortex surfaces. In terms

[8]Note that the mechanism generating fractional topological charge in the present context thus differs, e.g., from the topological charge fractionalization found using twisted boundary conditions on a torus, which does depend on the gauge group [45–47].

[9]Of course, for more than two colors, $N > 2$, more than one $SU(2)$ subgroup exists in which the gauge field can exhibit an Abelian magnetic monopole and the associated Dirac string; however, any given Dirac string in any specific $SU(2)$ subgroup of an $SU(N)$ group carries the same quantum of magnetic flux, independent of N.

of the reduced quantities[10]

$$q_{\mu\nu}(x) = \text{sgn Im Tr} \exp(2\pi i\, p_{\mu\nu}(x)/3) \;, \tag{11}$$

i.e., $q_{\mu\nu}(x) \in \{-1, 0, 1\}$, the action is

$$\begin{aligned} S \;\; = \;\; c \sum_x \sum_\mu \Bigg[\sum_{\substack{\nu<\lambda \\ \nu\neq\mu,\lambda\neq\mu}} & \left(|q_{\mu\nu}(x)\, q_{\mu\lambda}(x)| + |q_{\mu\nu}(x)\, q_{\mu\lambda}(x-e_\lambda)| \right. \\ & \left. + |q_{\mu\nu}(x-e_\nu)\, q_{\mu\lambda}(x)| + |q_{\mu\nu}(x-e_\nu)\, q_{\mu\lambda}(x-e_\lambda)| \right) \Bigg] \;. \end{aligned} \tag{12}$$

Thus, for every link in the lattice, the attached elementary squares carrying vortex flux are considered, and every instance of a pair of these squares not lying in the same plane costs an action increment c. The value of c,

$$c = 0.21 \tag{13}$$

is fixed [27] by demanding that the ratio of the deconfinement temperature to the square root of the zero temperature string tension reproduce the value obtained in $SU(3)$ Yang-Mills theory [48], $T_c/\sqrt{\sigma} = 0.63$.

Note, finally, that the lattice spacing is a fixed physical quantity, encoding the ultraviolet cutoff of this infrared effective model; physically, it implements the notion that vortices possess a finite transverse thickness. E.g., a pair of parallel thick vortices can only approach one another up to a minimal distance, below which their fluxes cease to be distinguishable from one another and should instead be represented as one combined flux with an appropriate new color orientation. It is therefore not meaningful to consider configurations in which two vortices run in parallel at a distance smaller than the aforementioned minimal one. This is reflected in the fixed lattice spacing used in conjunction with the hypercubic construction of the vortex world-surfaces. Fixing the scale by setting the zero-temperature string tension to $\sigma = (440\,\text{MeV})^2$, the lattice spacing takes the value $a = 0.39\,\text{fm}$, cf. [27].

4.2 Color structure

The action (12) contains no bias with respect to the color orientation of vortex flux. Also, the Bianchi identity only constrains the reduced quantities $q_{\mu\nu}(x)$, but does not distinguish between different color orientations of $p_{\mu\nu}(x)$ corresponding to the same $q_{\mu\nu}(x)$.

[10] Note that previous discussions of the $SU(3)$ random vortex world-surface model [27–29] were formulated directly in terms of the reduced variables $q_{\mu\nu}(x)$, since these are sufficient for encoding the values taken by Wilson loops in vortex configurations, and thus sufficient for the discussion of confinement properties, on which [27–29] focus. By contrast, for the discussion of topological properties, it is useful to introduce the more detailed specification of color orientation provided by the variables $p_{\mu\nu}(x)$ used in the present work. The space-time dynamics of the ensemble, depending only on the absolute values $|q_{\mu\nu}(x)|$, are unchanged.

This is in accordance with the fact that the color orientation of the (vortex) field strength can be locally rotated by gauge transformations in the underlying full Yang-Mills theory[11].

Nevertheless, it is necessary to make a specific choice of color orientation, i.e., of the full quantities $p_{\mu\nu}(x)$ for the purpose of evaluating the topological charge according to (9). In practice, vortex configurations are generated as in previous investigations of the $SU(3)$ random vortex world-surface model [27–29], i.e., in terms of $q_{\mu\nu}(x)$. Then, all vortex elementary squares are assigned random color orientations from the allowed set of T, cf. (6), consistent with the given $q_{\mu\nu}(x)$, thus arriving at an initial model description in terms of the full quantities $p_{\mu\nu}(x)$.

Before continuing, it should be emphasized that this assignment is not necessarily just a particular choice of gauge. Certainly, smooth local color rotations of the (vortex) field strength amount to gauge transformations, and one might therefore be tempted to regard a choice of $p_{\mu\nu}(x)$ for a given $q_{\mu\nu}(x)$ purely as a choice of gauge. However, while different choices of color orientation indeed fall into gauge equivalence classes, there is, in general, more than one class. Gauge-inequivalent choices are possible, in particular, at vortex intersection points: If one assigns color orientations to vortex world-surface elements completely independently, this also allows one to change the color orientation of one, but not the other, vortex surface meeting at the intersection point in question. This goes beyond what is possible using gauge transformations, which only allow one to rotate the entire gauge field strength present at a given point coherently. Thus, the assignment of color orientation to the vortex world-surfaces is related to, but not synonymous with a choice of gauge. Gauge-inequivalent $p_{\mu\nu}(x)$ for a given $q_{\mu\nu}(x)$ are possible, and these, in general, also differ in their topological charge. The topological charge can vary within certain bounds depending on the color orientation chosen for the configuration; it is not determined exclusively by the space-time location of the vortex world-surfaces.

It is thus certainly a relevant question to what extent the measurement of the topological susceptibility is biased by the way vortex color orientation is modeled. In order to glean some information regarding this issue, in practice, two alternative models are considered: Starting with the initial random assignment of color orientation in $p_{\mu\nu}(x)$ described above, sweeps through the lattice are performed in which the color orientations of individual elementary squares are changed with a bias towards either aligning or not aligning the orientations of adjacent squares; this corresponds to minimizing or maximizing the Abelian magnetic monopole density, respectively[12]. In this way, one arrives at alternative ensembles comprised of configurations $p^{min}_{\mu\nu}(x)$ and $p^{max}_{\mu\nu}(x)$, on both of

[11]Note that, in general, not all $p_{\mu\nu}(x)$ corresponding to the same $q_{\mu\nu}(x)$ are related by gauge transformations; this point will be revisited in more detail presently. Thus, the dynamics embodied in (12) are invariant not only under bona fide gauge transformations, but under a larger class of transformations connecting all possible color orientations of the vortex field strength.

[12]The, in general, nonorientable nature of the vortex world-surfaces implies a lower bound on the monopole density achievable in this way, while the lattice spacing provides an upper cutoff.

which topological charge is measured (after removing the lattice ambiguities discussed in section 3.2). While the two ensembles will be seen to differ widely in monopole density, the results obtained in either case for the topological susceptibility exhibit only minor deviations from each other. To this extent, thus, an unambiguous prediction of the topological susceptibility emerges despite the freedom one has in modeling vortex color orientation. The reason for this lies in the fact that the topological charge of generic vortex world-surfaces is dominated by vortex writhe, as will be seen in more detail in section 5.2. Vortex intersections, at which gauge-inequivalent color orientation choices leading to differing topological charge are possible, cf. the discussion further above, by contrast only generate a minor contribution to the overall vortex topological charge. Note that entirely analogous observations were already made in the $SU(2)$ random vortex world-surface model, cf. [25].

5 Numerical results and discussion

5.1 Measurement parameters

Measurements were carried out at the physical value of the curvature coefficient, $c = 0.21$, on $12^3 \times N_t$ lattices, variation of N_t permitting the study of a collection of temperatures including both the confined as well as the deconfined phases. Note that a spatial extent of 12 lattice spacings corresponds to 4.7 fm; this is sufficiently large compared to typical strong interaction scales to render finite size effects insignificant. Furthermore, in order to obtain more closely spaced data as a function of temperature than provided by the direct measurements at $c = 0.21$, the following interpolation procedure was used in addition: A determination [29] of the critical values of c at which the deconfinement transition occurs for $N_t = 1, 2, 3$, cf. Table 1, yields $aT_c = 1/N_t$ for those values of c. An interpolating

N_t	1	2	3
c	0.0872	0.2359	0.335

Table 1: Critical values of the curvature coefficient c at which the deconfining phase transition occurs.

parabola in c then defines aT_c for a continuous range of c (in particular, $aT_c = 0.5655$ for $c = 0.21$, i.e., a $N_t = 1$ lattice corresponds to $T/T_c = 1.77$ at the physical value of c). On this basis, then, $T/T_c = 1/(N_t \cdot aT_c(c))$ is defined for any combination of c, N_t. Now, one can perform measurements at a given fixed value of T/T_c for different N_t and the corresponding c. Interpolating the results as a function of c to the physical point $c = 0.21$ finally yields the desired supplementary data at the chosen T/T_c. Table 2 lists the additional combinations of N_t and c at which measurements were performed for use

T/T_c	$N_t = 1$	$N_t = 2$	$N_t = 3$
0.98	0.082565	0.23162	0.32854
1.02	0.09172	0.24012	0.3418
1.1	0.10872	0.25642	–
1.4	0.16102	0.3143	–

Table 2: Temperatures and corresponding curvature coefficients c at which measurements were performed for $N_t = 1, 2, 3$, to supplement the direct measurements at $c = 0.21$.

in the above interpolation procedure; note that only values of c inside, or very close to the range covered by the critical values listed in Table 1 were used, in order to preclude extrapolation instabilities. As a consequence, the final interpolation to $c = 0.21$ relies on three data points in the cases of $T/T_c = 0.98$ and $T/T_c = 1.02$, whereas it relies on two data points in the other two cases.

In practice, the numerical results discussed below were generated using about $400000/N_t$ samples for each measurement; as N_t is raised, increased volume averaging implies that correspondingly fewer configurations are needed to arrive at a similar statistical accuracy. Samples were taken separated by 50 Monte Carlo sweeps through the lattice; since the bulk of the computational effort lies in the evaluation of the topological charge, even this substantial number of decorrelating steps constitutes only a minor contribution to the overall cost.

5.2 Numerical results

The results for the topological susceptibility $\chi = \langle Q^2 \rangle / V$ (where V denotes the space-time four-volume) are given in Tables 3 and 4, the former referring to the ensemble with minimized Abelian monopole density, cf. the discussion in section 4.2, the latter referring to the ensemble with maximized Abelian monopole density. For both cases, besides the total topological susceptibility χ, also the susceptibility χ_{int} resulting from counting only the contributions from vortex world-surface intersection points[13] is quoted. Furthermore, the Abelian magnetic monopole density $\rho_{monop} = L_{monop}/V$ (evaluated before applying the algorithms removing the ambiguities discussed in section 3.2) is given, where L_{monop} is the monopole world-line length present in the configuration (normalized such that a single monopole world-line occupying a lattice link contributes a length a). Finally, the aforementioned algorithms, removing hypercubic lattice surface ambiguities in order to make an unambiguous evaluation of the topological charge possible, cf. section 3.2, involve local deformations of the vortex world-surfaces; this, however, leads to

[13]Note that counting only contributions from intersection points leads to a topological charge Q_{int} quantized in units of 1/3.

T/T_c	$\chi^{1/4}$/MeV	$\chi_{int}^{1/4}$/MeV	$\rho_{monop} \cdot \mathrm{fm}^3$	ρ_{def}/ρ_{orig}
0.15	222	98	12.6	1.39
0.29	222	98	12.6	1.39
0.44	222	98	12.6	1.39
0.59	222	98	12.5	1.39
0.88	221	100	11.9	1.39
0.98	222	105	11.0	1.40
1.02	209	102	9.41	1.38
1.1	189	99	6.42	1.39
1.4	156	92	3.25	1.43
1.77	150	93	1.96	1.47

Table 3: Numerical results for ensemble with minimized magnetic monopole density. Statistical uncertainties are smaller than the accuracy to which quantities are quoted. The various columns are explained in detail in the main text.

an appreciable increase in the vortex world-surface density. The ratio of the deformed world-surface density ρ_{def} to the original density ρ_{orig} is reported in the final column in Tables 3 and 4; these data are the same in the two tables, since the ensembles in question differ exclusively in the choice of color structure, whereas the space-time locations of the vortices are identical.

Evidently, the ensembles with minimized and maximized monopole densities, respectively, differ considerably in color structure, as quantified by those densities. Yet, the differences in the topological susceptibilities measured in the two cases are minor, increasing slightly at high temperatures. To this extent, the prediction for the topological susceptibility obtained in the $SU(3)$ random vortex world-surface model is unambiguous as far as the modeling of vortex color structure is concerned. The reason for this behavior lies in the space-time structure of generic world-surface configurations. As seen in Tables 3 and 4, the topological susceptibility induced by world-surface intersection points alone is much smaller than the contribution from vortex writhe; even when considering the fourth root, $\chi^{1/4}$ and $\chi_{int}^{1/4}$ still differ roughly by a factor of two. Vortex writhe is the dominant mechanism by which center vortices generate topological charge. However, the contribution from vortex writhe is explicitly invariant under color rotations of the vortex field strength, since only one world-surface is involved in generating such contributions. Only vortex intersection points involve two distinct surfaces, independent color rotations of which can lead to gauge-inequivalent color configurations, and thus change topological charge. The relative paucity of such intersection points in generic world-surface configurations, as evidenced by the magnitude of χ_{int}, explains the very similar results for the topological susceptibility obtained in the two ensembles investigated, despite their

T/T_c	$\chi^{1/4}$/MeV	$\chi_{int}^{1/4}$/MeV	$\rho_{monop} \cdot \mathrm{fm}^3$	ρ_{def}/ρ_{orig}
0.15	224	98	63.2	1.39
0.29	223	98	63.2	1.39
0.44	223	98	63.2	1.39
0.59	223	99	63.2	1.39
0.88	223	101	63.4	1.39
0.98	223	107	61.7	1.40
1.02	210	105	58.0	1.38
1.1	191	104	47.1	1.39
1.4	161	98	30.9	1.43
1.77	156	98	23.5	1.47

Table 4: Numerical results for ensemble with maximized magnetic monopole density. Statistical uncertainties are smaller than the accuracy to which quantities are quoted. The various columns are explained in detail in the main text.

considerably differing color structure.

The results for the topological susceptibility summarized in Tables 3 and 4 suffer from one significant systematic uncertainty. Namely, as discussed in section 3.2, an unambiguous evaluation of the topological charge of a hypercubic vortex world-surface configuration only becomes possible after an algorithm is applied during which the configurations are placed on finer lattices and subjected to suitable local deformations. These deformations appreciably increase the vortex density, as evidenced by the ratio ρ_{def}/ρ_{orig} reported in Tables 3 and 4. In general, in the process, also spurious additional topological charge density will be generated concomitantly on the finer lattices. To obtain a rough estimate of this effect, by simply counting dimensions, the topological susceptibility would be expected to scale with the square of the vortex world-surface density (a critique of this estimate is given below). On this basis, an estimate for the amount by which the raw data for the fourth root of the topological susceptibility given in Tables 3 and 4 may need to be systematically revised downward, to offset the effects of the deformation procedure, can be obtained by dividing those data by the square root of the ratio ρ_{def}/ρ_{orig}. This yields the lower ends of the error bars depicted in Fig. 6, which, for definiteness, shows the results obtained from the ensemble with minimized magnetic monopole density.

One may alternatively contemplate interpreting the lower ends of the error bars in Fig. 6 not merely as estimates of a systematic uncertainty, but as appropriately adjusted data in their own right, akin to renormalized quantities. Of course, this is mainly a metaphorical interpretation, since no systematic scheme has been developed within the present infrared effective model which would allow one to quantify the dependence on the

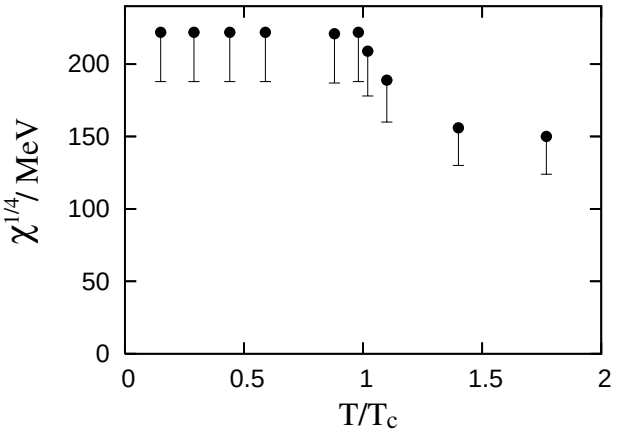

Figure 6: Fourth root of the topological susceptibility measured in the $SU(3)$ random vortex world-surface model, as a function of temperature. The results from the ensemble with minimized Abelian magnetic monopole density are depicted. Statistical uncertainties of the data are smaller than the filled circle symbols displaying the measured values; the downward uncertainty shown is a systematic one, discussed in detail in the main text.

lattice spacing. However, on the finer lattices on which the deformations of the vortex world-surfaces and the ensuing evaluation of their topological charge are performed, presumably a suitably renormalized effective action exists which would directly generate the deformed world-surfaces if one worked from the very beginning on those finer lattices. The measurement of the topological susceptibility is carried out on the finer lattice, in the ensemble controlled by the corresponding renormalized action. Thus, it seems plausible that translating the measurement back to the original scale should be accompanied by a suitable renormalization, and that it is in principle appropriate to discuss the results in terms of corresponding renormalized quantities. Of course, the rescaling by the density ratio ρ_{def}/ρ_{orig} employed here is no more than a rough phenomenological estimate of this renormalization; after all, the fluctuations of the vortex world-surfaces engendered by their local deformation on the finer lattices, while to a certain extent random, are not governed by a simple curvature action of the form (12), and therefore one must expect corrections to the simple scaling with the vortex density. These caveats must be kept in mind in the context of interpreting the rescaled topological susceptibility as a physical quantity in its own right.

Comparing to the $SU(2)$ random vortex world-surface model studied in [25], the modifications of the world-surfaces in the course of the deformation algorithm, as quantified by the density ratio ρ_{def}/ρ_{orig}, become stronger as one progresses to $SU(3)$. At low temperatures, $\rho_{def}/\rho_{orig} = 1.39$ in the $SU(3)$ model, whereas one has only $\rho_{def}/\rho_{orig} = 1.19$ for $SU(2)$. Similarly, in the deconfined phase, the ratio rises to $\rho_{def}/\rho_{orig} = 1.47$ at $T = 1.77\,T_c$ in the $SU(3)$ model, whereas, in the $SU(2)$ model at $T = 1.66\,T_c$, one finds

$\rho_{def}/\rho_{orig} = 1.20$. This behavior is plausible in view of the fact that $SU(3)$ vortices each carry less chromomagnetic flux than $SU(2)$ vortices. As a consequence, a given amount of flux will be fragmented into more world-surface area in the $SU(3)$ case. Indeed, this is borne out by the data: In the $SU(2)$ model, at low temperatures, 27% of elementary squares in the lattice carry vortex flux (on the original coarse lattice, before deformation); by contrast, in the $SU(3)$ model, this rises to 36% of elementary squares. It seems plausible that, the higher the percentage of occupied squares, the more elaborate the deformations necessary to eliminate all world-surface ambiguities become. Hence, the enhanced ρ_{def}/ρ_{orig} ratio for $SU(3)$ as compared to $SU(2)$.

In terms of the topological susceptibility[14], the raw data for the $SU(3)$ vortex model are considerably higher than for the $SU(2)$ model[15] investigated in [25]; namely, at low temperatures, $\chi^{1/4}_{raw} = 222\,\mathrm{MeV}$ for $SU(3)$ vs. $\chi^{1/4}_{raw} = 190\,\mathrm{MeV}$ for $SU(2)$. Here and in the following, $\chi^{1/4}_{raw}$ simply denotes the measured data labeled as $\chi^{1/4}$ in Table 3 and displayed by the filled circles in Fig. 6; on the other hand, the data rescaled with ρ_{def}/ρ_{orig} as discussed above, corresponding to the lower ends of the error bars displayed in Fig. 6, will be denoted by $\chi^{1/4}_{rescaled}$, i.e., $\chi^{1/4}_{rescaled} = \chi^{1/4}_{raw}/\sqrt{\rho_{def}/\rho_{orig}}$. In terms of the rescaled quantities, the comparison between the $SU(3)$ and $SU(2)$ models at low temperatures is much closer, although the $SU(3)$ result still lies above the $SU(2)$ one, namely, $\chi^{1/4}_{rescaled} = 188\,\mathrm{MeV}$ vs. $\chi^{1/4}_{rescaled} = 174\,\mathrm{MeV}$. At high temperatures, the contrast is stronger: In the $SU(3)$ model at $T = 1.77\,T_c$, one has $\chi^{1/4}_{raw} = 150\,\mathrm{MeV}$, whereas the $SU(2)$ model at $T = 1.66\,T_c$ yields $\chi^{1/4}_{raw} = 109\,\mathrm{MeV}$. On the other hand, in terms of the rescaled quantities at the same temperatures, $\chi^{1/4}_{rescaled} = 124\,\mathrm{MeV}$ for $SU(3)$, while $\chi^{1/4}_{rescaled} = 100\,\mathrm{MeV}$ for $SU(2)$. These comparisons will be revisited below in relation to corresponding lattice Yang-Mills results.

5.3 Comparison to lattice Yang-Mills theory

Lattice Yang-Mills results for the $SU(3)$ topological susceptibility have been reported in a number of works, cf., e.g., [49–58], and reviewed in [59]; cf. the latter also for a much more extensive list of related studies. There is a considerable spread in the reported results, obtained using various methods, with values as high as $\chi^{1/4} = 213(7)\,\mathrm{MeV}$ and as low as $\chi^{1/4} = 168(11)\,\mathrm{MeV}$ obtained at zero temperature in the last decade, cf. Table 1 in [59]. The corresponding raw data at low temperatures found in the $SU(3)$ random vortex world-surface model lie somewhat above this range, at $\chi^{1/4}_{raw} = 222\,\mathrm{MeV}$. On the other hand, the rescaled result, $\chi^{1/4}_{rescaled} = 188\,\mathrm{MeV}$, lies near the center of the range of lattice Yang-Mills data; the vortex model results thus appear compatible with the lattice

[14]For definiteness, the discussion in the remainder of this section and also in the next section will refer specifically to the results obtained in the ensemble with minimized Abelian magnetic monopole density, cf. Table 3.

[15]The comparison between $SU(3)$ and $SU(2)$ is performed on the basis of positing an identical zero-temperature string tension, $\sigma(T = 0) = (440\,\mathrm{MeV})^2$, to set the scale in both cases.

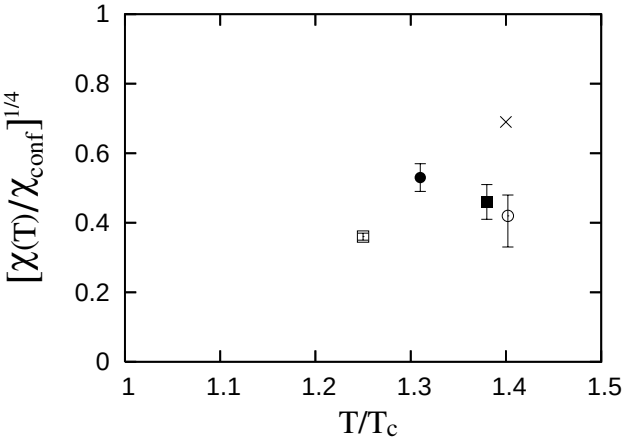

Figure 7: Ratio of the topological susceptibility at a temperature T above the deconfinement transition to the topological susceptibility in the confined phase, from various $SU(3)$ lattice Yang-Mills calculations and the present vortex model. Fourth root of the ratio is shown, as a function of T/T_c. Open circle depicts data from [49], filled circle data from [50], open square data from [51], and filled square data from [52] complemented by information from [51], cf. discussion in main text. In the former three cases, uncertainties are estimated from error bars given in the corresponding publications, in the latter case, from comparison of results obtained on lattices of different sizes, which make an error estimate of about 10% seem appropriate. Finally, the "x" symbolizes the vortex model result; in this case, statistical uncertainties are negligible. The vortex model result appears to remain appreciably above the lattice results; possible systematic effects leading to this deviation are discussed in section 6.

Yang-Mills results at low temperatures.

Continuing to finite temperature, above the deconfining phase transition, the topological susceptibility is seen to fall off rapidly with temperature in $SU(3)$ lattice Yang-Mills theory [49–52]. Quantitatively, [49] reports a drop in $\chi^{1/4}$ by a factor 2.4 as the temperature is raised from $T = 0.834\,T_c$ to $T = 1.402\,T_c$; [50] reports a drop in $\chi^{1/4}$ by a factor 1.9 as the temperature is raised from $T = 0.88\,T_c$ to $T = 1.31\,T_c$. An even stronger suppression is reported by [51], namely, by a factor 2.8 as the temperature rises from just below the deconfinement temperature, $T = 0.99\,T_c$, up to $T = 1.25\,T_c$. This seems significantly different from the former two measurements, which appear compatible with each other. Finally, [52] gives only data in the deconfined phase, reporting a drop in $\chi^{1/4}$ by a factor 1.9 as the temperature is raised from just above the transition, $T = 1.03\,T_c$, to $T = 1.38\,T_c$ (using the data obtained on $16^3 \times 4$ lattices quoted in [52]). If one combines this with data on the discontinuity across the deconfining phase transition [51], indicating a drop in $\chi^{1/4}$ by an additional factor 1.15 across the transition, this cumulatively amounts to a drop in $\chi^{1/4}$ by a factor 2.2 as one increases the temperature from the confined phase up to $T = 1.38\,T_c$. This again seems compatible with the results

from [49,50]. These lattice Yang-Mills data are also summarized in Fig. 7, along with the result obtained in the $SU(3)$ random vortex world-surface model for comparison. Also in the $SU(3)$ random vortex world-surface model, the topological susceptibility quickly becomes suppressed in the deconfined phase as temperature rises, cf. Fig. 6; however, quantitatively, the suppression is not as strong as the one seen in $SU(3)$ lattice Yang-Mills theory. The raw topological susceptibility data in Table 3 show a drop in $\chi_{raw}^{1/4}$ from $\chi_{raw}^{1/4} = 221\,\mathrm{MeV}$ to $\chi_{raw}^{1/4} = 156\,\mathrm{MeV}$, i.e., by a factor 1.42, as the temperature is raised from $T = 0.88\,T_c$ to $T = 1.4\,T_c$. This does not change substantially when the rescaled data are considered, since the density ratio ρ_{def}/ρ_{orig} does not vary strongly with temperature; in terms of rescaled data, $\chi_{rescaled}^{1/4}$ drops by a factor 1.44 in the same temperature range. Thus, the topological susceptibility found in the $SU(3)$ random vortex world-surface model in the deconfined phase does appear to remain appreciably above the corresponding lattice Yang-Mills results. The comparison with lattice Yang-Mills theory in the present $SU(3)$ case in the deconfined phase therefore is less favorable than for the previously studied $SU(2)$ model [25], which is quantitatively compatible with corresponding lattice Yang-Mills results even above the deconfining transition. Possible causes of this will be discussed in the next section.

Another way to cast the comparison between the random vortex world-surface model and lattice Yang-Mills theory is in terms of the trend, already alluded to at the end of the previous section, as one progresses from the $SU(2)$ to the $SU(3)$ gauge group. This in fact yields the starkest contrast. In lattice Yang-Mills theory, at low temperatures, the topological susceptibility is expected to fall as the number of colors N is increased [59]. The preponderance of evidence points to this already being the case as one goes from $SU(2)$ to $SU(3)$ [51, 53–55], although it should be noted that agreement on this only emerges when the results are extrapolated to vanishing lattice spacing [53, 55]; at finite lattice spacing, a slight increase of the zero-temperature topological susceptibility going from $SU(2)$ to $SU(3)$ has been seen [51, 53]. A detailed discussion of the continuum extrapolation can be found in [53]. Disregarding these details, in the confined phase, the lattice Yang-Mills topological susceptibilities found in the $SU(2)$ and $SU(3)$ cases only differ mildly. In this respect, the random vortex world-surface model can still be viewed as compatible with lattice Yang-Mills theory; as already observed at the end of the previous section, while the raw topological susceptibility data obtained at low temperatures in the $SU(3)$ and $SU(2)$ cases differ substantially, $\chi_{raw}^{1/4} = 222\,\mathrm{MeV}$ for $SU(3)$ vs. $\chi_{raw}^{1/4} = 190\,\mathrm{MeV}$ for $SU(2)$, in terms of the rescaled quantities, the $SU(3)$ result only lies slightly above the $SU(2)$ result, namely, $\chi_{rescaled}^{1/4} = 188\,\mathrm{MeV}$ vs. $\chi_{rescaled}^{1/4} = 174\,\mathrm{MeV}$.

The picture changes qualitatively as one crosses into the deconfined phase. While the vortex model does display a strong drop in the topological susceptibility both for $SU(3)$ and $SU(2)$ as the temperature is raised, as already discussed further above, the suppression seen is substantially stronger for $SU(2)$ than for $SU(3)$, even in terms of the rescaled quantities. In the $SU(3)$ model at $T = 1.77\,T_c$, one has $\chi_{rescaled}^{1/4} = 124\,\mathrm{MeV}$,

whereas already at $T = 1.66\,T_c$, the $SU(2)$ model yields $\chi^{1/4}_{rescaled} = 100\,\mathrm{MeV}$. This does seem clearly at odds with the behavior seen in lattice Yang-Mills theory. There, all evidence points towards the reverse relation[16]: [56] shows (cf. Fig. 4 therein), at $T = 1.3\,T_c$, a $SU(3)$ topological susceptibility which is smaller by roughly a factor 10 compared to the $SU(2)$ susceptibility; in terms of the fourth root, $\chi^{1/4}$, this means a suppression of the $SU(3)$ result compared to the $SU(2)$ result by a factor 1.8 at $T = 1.3\,T_c$. Also [52] reports data for both $SU(3)$ at $T = 1.38\,T_c$, and for $SU(2)$ at $T = 1.4\,T_c$. The data are in lattice units; using the results obtained in [52] at the aforementioned temperatures on $16^3 \times 4$ lattices, one has $(\chi[SU2]/\chi[SU3]) \cdot (a[SU(2)]/a[SU(3)])^4 = 5.1$ at roughly $T = 1.4\,T_c$. One can convert to physical units, e.g., by observing that $T_c a$ is roughly the same in both measurements; then, using $T_c/\sqrt{\sigma} = 0.69$ for $SU(2)$ and $T_c/\sqrt{\sigma} = 0.63$ for $SU(3)$ (σ denoting the zero-temperature string tension), this implies that $a[SU(2)]/a[SU(3)] = 0.9$. Taken together, therefore, at roughly $T = 1.4\,T_c$, the $SU(3)$ result for $\chi^{1/4}$ is suppressed compared to the $SU(2)$ result by a factor 1.67, similar to the behavior shown in [56]. Thus, in the deconfined phase, substantial disagreement is seen between the random vortex world-surface model and lattice Yang-Mills theory, as far the comparison between the topological susceptibilities obtained in the $SU(3)$ and $SU(2)$ cases is concerned.

6 Outlook

The results presented and discussed in the previous section indicate that the topological properties of the $SU(3)$ random vortex world-surface model investigated in this work are consistent with $SU(3)$ Yang-Mills theory in the confined phase. However, in the deconfined phase, while the vortex model does qualitatively exhibit a strong suppression of the topological susceptibility as temperature is raised, on a quantitative level, this suppression is significantly less abrupt than the one found in $SU(3)$ lattice Yang-Mills measurements. This stands in contrast to the $SU(2)$ random vortex world-surface model investigated previously [25], which is quantitatively compatible with the corresponding $SU(2)$ Yang-Mills theory even in the deconfined phase. At this point, not sufficient information is available to pinpoint the source of the discrepancy found in the $SU(3)$ case. Possible causes are the following:

The discrepancy may be an artefact of the hypercubic description, which, as discussed in section 3.2, engenders a significant systematic uncertainty in the determination of the topological charge. Indeed, this uncertainty is considerably larger in the $SU(3)$ case than in the $SU(2)$ case, as evidenced by the change of vortex density in the course of the vortex world-surface deformations applied, cf. section 3.2, in order to remove ambiguities in the surfaces. Essentially, the constraint implied by the hypercubic description, namely, that only six discrete space-time planes are available in which world-surfaces can extend,

[16] Indeed, one expects the topological susceptibility to vanish in the deconfined phase as $N \to \infty$ [59].

is considerably more stringent in the $SU(3)$ model. Since vortex flux is fragmented into smaller units in the $SU(3)$ case, already to begin with, a higher proportion of lattice elementary squares is occupied by vortex flux; this makes it correspondingly more difficult to find deformations of the surfaces, within the restricted set of space-time planes, suited to remove surface ambiguitites. Further to this issue, it should also be recognized that the topologies of the surfaces qualitatively differ for $SU(3)$ and $SU(2)$; only the former permits vortex branching. As a result, comparing the behavior of the world-surface ambiguities in the two cases is not straightforward; it is entirely possible that the rough phenomenological prescription applied in section 5.2 to estimate the systematic uncertainty, namely, scaling by the appropriate power of ρ_{def}/ρ_{orig}, is subject to sizeable corrections which may behave very differently for $SU(3)$ and $SU(2)$. It should again be emphasized that the aforementioned effects are not generic to the random vortex world-surface concept, but are introduced by the specific hypercubic construction of the world-surfaces. More comments follow below on how this limitation may be circumvented.

To the extent that artefacts of the hypercubic description do not account for the discrepancies compared to Yang-Mills theory observed in the deconfined phase, several physical causes are possible. For one, as one raises the temperature past the deconfining phase transition and further into the deconfined phase, one rapidly approaches the ultra-violet cutoff of the model. This may appreciably distort the results (again, in a fashion which may differ considerably for the $SU(3)$ and $SU(2)$ cases due to the qualitatively different topology of the world-surfaces). The good agreement with lattice Yang-Mills theory found for $SU(2)$ at high temperatures could, in this context, be coincidental to an extent.

Furthermore, the pure vortex world-surface curvature action employed in the model investigated here may not completely capture all relevant dynamics. Indeed, on general grounds, one expects a shift in the dynamical characteristics of center vortices as the number of colors N in the underlying Yang-Mills theory is raised [60]. The necessity for such a shift, moreover, was observed explicitly in the $SU(4)$ random vortex world-surface model investigated in [30]. There, already the confinement properties of the corresponding Yang-Mills theory could only be reproduced by introducing new terms into the effective vortex action beyond a pure world-surface curvature term. In the present $SU(3)$ case, the confinement properties obtained using a pure world-surface curvature action still do not differ significantly from $SU(3)$ Yang-Mills theory, cf. [27–29]. Possibly, the topological susceptibility investigated in the present work is more sensitive to the details of the vortex dynamics, and the discrepancy compared to $SU(3)$ Yang-Mills theory observed at high temperatures may thus signal the need for an adjustment of the effective vortex dynamics already for $SU(3)$.

One possibility which comes to mind in this respect is the inclusion of explicit action terms for thickened monopole world-lines residing on the vortex world-surfaces. Variational estimates for the energies of various monopole-type objects have been given in [40];

the objects referred to as "monopoles" in the present work correspond to the "fully non-Abelian nexi" of [40]. It is argued there that $SU(3)$ monopoles have considerably higher energy than $SU(2)$ monopoles. This mechanism would therefore be consistent with the phenomena observed in the random vortex world-surface model in more than one way: On the one hand, it seems plausible that the deconfined phase is less entropy-dominated than the confined phase, since the former is, effectively, dimensionally reduced compared to the latter. Thus, one would expect the energetics of, say, monopoles to be more relevant in the deconfined phase, where, indeed, the discrepancies compared to Yang-Mills theory are observed. Furthermore, if $SU(3)$ monopoles imply a much larger action penalty than $SU(2)$ monopoles, this would simultaneously explain why the discrepancies are only observed in the $SU(3)$ model and not the $SU(2)$ model. Finally, the fact that monopoles are intimately tied to the topological properties of vortex world-surfaces (by encoding their non-orientedness) would seem consistent with the discrepancies becoming apparent specifically in the topological susceptibility.

It would certainly be useful to be able to discriminate between the different possible sources of the deviation observed at high temperatures between the $SU(3)$ random vortex world-surface model studied here and $SU(3)$ Yang-Mills theory. In particular, it would be interesting to distinguish whether this deviation is an artefact of the hypercubic construction of the world-surfaces or whether it has a more physical origin. To this end, an alternative formulation in terms of random triangulations offers itself, with a minimal area of the triangles serving as the ultraviolet cutoff. By providing a continuum of directions into which the vortex surfaces can extend, the most pernicious world-surface ambiguities discussed in section 3.2 would be avoided from the outset; intersections between surfaces would generically occur at isolated space-time points. This would obviate the need to transfer configurations to a finer scale and perform deformations, thus avoiding the associated renormalization uncertainties. The topological charge can be well defined at the original scale in such a formulation. The drawback of a construction in terms of triangulations is that book-keeping of vortex locations is considerably more unwieldy, raising questions concerning, e.g., appropriate rules for dynamically disconnecting and fusing world-surfaces. Given that the deconfining phase transition is a percolation transition, such processes play a crucial role in the vortex picture.

A complementary line of investigation which would mitigate some of the artefacts engendered by the hypercubic construction, without abandoning it altogether, lies in evaluating the index of the Dirac operator in the model vortex ensemble. This can be achieved without transferring vortex configurations to finer lattices, thus again avoiding the associated renormalization uncertainties. On the other hand, it must be emphasized that, in light of the discussion in section 3.3, the generalization of the index theorem to generic vortex configurations is not obvious. Since the configurations are defined on manifolds with a complicated, dynamic topology, corrections to the index theorems valid on simple manifolds such as spheres or tori must be expected; this already manifests

itself in the fractionalization of global topological charge found for the model vortex configurations studied here. It would certainly be interesting to study the correlation between the topological charge and the Dirac operator index in the vortex ensemble. A construction of the Dirac operator in the context of the $SU(2)$ vortex world-surface model has been given in [26], albeit discarding the exact zero-mode sector (which is irrelevant for the chiral condensate discussed there). A suitable generalization permitting the study of the spectral flow of that type of operator is needed in order to access the Dirac operator index.

Finally, on a more formal level, it would be interesting to understand the extent to which the specific half-integer quantization of global topological charge observed for the model vortex configurations investigated in this work is determined by the hypercubic description. Surfaces composed of elementary squares in hypercubic fashion only constitute a particular subset of continuum surfaces in four dimensions; further fractionalization of topological charge for more general surfaces is conceivable. This more general case remains to be explored.

Acknowledgments

This work was supported by the U.S. DOE under grant number DE-FG02-96ER40965.

References

[1] G. 't Hooft, Nucl. Phys. **B138** (1978) 1.

[2] Y. Aharonov, A. Casher and S. Yankielowicz, Nucl. Phys. **B146** (1978) 256.

[3] J. M. Cornwall, Nucl. Phys. **B157** (1979) 392.

[4] G. Mack and V. B. Petkova, Ann. Phys. (NY) **123** (1979) 442.

[5] G. Mack, Phys. Rev. Lett. **45** (1980) 1378.

[6] G. Mack and V. B. Petkova, Ann. Phys. (NY) **125** (1980) 117.

[7] G. Mack and E. Pietarinen, Nucl. Phys. **B205** [FS5] (1982) 141.

[8] H. B. Nielsen and P. Olesen, Nucl. Phys. **B160** (1979) 380.

[9] J. Ambjørn and P. Olesen, Nucl. Phys. **B170** [FS1] (1980) 60.

[10] J. Ambjørn and P. Olesen, Nucl. Phys. **B170** [FS1] (1980) 265.

[11] P. Olesen, Nucl. Phys. **B200** [FS4] (1982) 381.

[12] E. T. Tomboulis, Phys. Rev. D **23** (1981) 2371.

[13] J. Greensite, Prog. Part. Nucl. Phys. **51** (2003) 1.

[14] M. Engelhardt, Nucl. Phys. Proc. Suppl. **140** (2005) 92.

[15] L. Del Debbio, M. Faber, J. Greensite and Š. Olejník, Phys. Rev. D **55** (1997) 2298.

[16] L. Del Debbio, M. Faber, J. Giedt, J. Greensite and Š. Olejník, Phys. Rev. D **58** (1998) 094501.

[17] C. Alexandrou, M. D'Elia and P. de Forcrand, Nucl. Phys. Proc. Suppl. **83** (2000) 437.

[18] M. Engelhardt, K. Langfeld, H. Reinhardt and O. Tennert, Phys. Rev. D **61** (2000) 054504.

[19] P. de Forcrand and M. D'Elia, Phys. Rev. Lett. **82** (1999) 4582.

[20] R. Bertle, M. Engelhardt and M. Faber, Phys. Rev. D **64** (2001) 074504.

[21] R. Höllwieser, M. Faber, J. Greensite, U. Heller and Š. Olejník, Phys. Rev. D **78** (2008) 054508.

[22] A. Kovalenko, S. Morozov, M. Polikarpov and V. Zakharov, Phys. Lett. **B648** (2007) 383.

[23] E.-M. Ilgenfritz, K. Koller, Y. Koma, G. Schierholz, T. Streuer, V. Weinberg and M. Quandt, PoS **LAT2007** (2007) 311.

[24] M. Engelhardt and H. Reinhardt, Nucl. Phys. **B585** (2000) 591.

[25] M. Engelhardt, Nucl. Phys. **B585** (2000) 614.

[26] M. Engelhardt, Nucl. Phys. **B638** (2002) 81.

[27] M. Engelhardt, M. Quandt and H. Reinhardt, Nucl. Phys. **B685** (2004) 227.

[28] M. Engelhardt, Phys. Rev. D **70** (2004) 074004.

[29] M. Quandt, H. Reinhardt and M. Engelhardt, Phys. Rev. D **71** (2005) 054026.

[30] M. Engelhardt, Phys. Rev. D **73** (2006) 034015.

[31] M. Engelhardt and B. Sperisen, Phys. Rev. D **74** (2006) 125011.

[32] F. Bruckmann, E.-M. Ilgenfritz, B. Martemyanov and B. Zhang, Phys. Rev. D **81** (2010) 074501.

[33] G. Jordan, R. Höllwieser, M. Faber and U. Heller, Phys. Rev. D **77** (2008) 014515.

[34] R. Höllwieser, M. Faber and U. Heller, eprint arXiv:1005.1015.

[35] M. Engelhardt, PoS **LATTICE2008** (2008) 253.

[36] M. Engelhardt, PoS **Confinement8** (2008) 055.

[37] M. Faber, J. Greensite and Š. Olejník, Phys. Rev. D **57** (1998) 2603.

[38] J. Greensite, K. Langfeld, Š. Olejník, H. Reinhardt and T. Tok, Phys. Rev. D **75** (2007) 034501.

[39] M. Engelhardt and H. Reinhardt, Nucl. Phys. **B567** (2000) 249.

[40] J. M. Cornwall, Phys. Rev. D **58** (1998) 105028.

[41] J. M. Cornwall, Phys. Rev. D **61** (2000) 085012.

[42] J. M. Cornwall, Phys. Rev. D **65** (2002) 085045.

[43] J. M. Cornwall and N. Graham, Phys. Rev. D **66** (2002) 065012.

[44] F. Bruckmann and M. Engelhardt, Phys. Rev. D **68** (2003) 105011.

[45] G. 't Hooft, Nucl. Phys. **B153** (1979) 141.

[46] P. van Baal, Comm. Math. Phys. **85** (1982) 529.

[47] P. de Forcrand and L. von Smekal, Phys. Rev. D **66** (2002) 011504.

[48] G. Boyd, J. Engels, F. Karsch, E. Laermann, C. Legeland, M. Lütgemeier and B. Petersson, Nucl. Phys. **B469** (1996) 419.

[49] B. Allés, M. D'Elia and A. Di Giacomo, Nucl. Phys. **B494** (1997) 281; erratum ibid. **B679** (2004) 397.

[50] C. Gattringer, R. Hoffmann and S. Schaefer, Phys. Lett. **B535** (2002) 358.

[51] B. Lucini, M. Teper and U. Wenger, Nucl. Phys. **B715** (2005) 461.

[52] R. Edwards, U. Heller, J. Kiskis and R. Narayanan, Nucl. Phys. Proc. Suppl. **83** (2000) 479.

[53] B. Lucini and M. Teper, JHEP **0106** (2001) 050.

[54] N. Cundy, M. Teper and U. Wenger, Phys. Rev. D **66** (2002) 094505.

[55] P. de Forcrand, M. García Pérez, J. Hetrick and I.-O. Stamatescu, in: Proceedings of the 31st International Ahrenshoop Symposium on the Theory of Elementary Particles, Buckow, Germany, Sept. 2–6, 1997, eds.: H. Dorn, D. Lüst and G. Weigt; Wiley-VCH, Berlin 1998; eprint hep-lat/9802017.

[56] B. Allés, M. D'Elia and A. Di Giacomo, Phys. Lett. **B412** (1997) 119.

[57] L. Del Debbio, L. Giusti and C. Pica, Phys. Rev. Lett. **94** (2005) 032003.

[58] S. Dürr, Z. Fodor, C. Hoelbling and T. Kurth, JHEP **0704** (2007) 055.

[59] E. Vicari and H. Panagopoulos, Phys. Rept. **470** (2009) 93.

[60] J. Greensite and Š. Olejník, JHEP **0209** (2002) 039.